The Journal of Chemical Physics

A comparative study of structural, electronic, and optical properties of thiolated gold clusters with icosahedral vs face-centered cubic cores

Cite as: J. Chem. Phys. **155**, 094304 (2021); https://doi.org/10.1063/5.0057566
Submitted: 22 May 2021 • Accepted: 17 August 2021 • Published Online: 02 September 2021

Maho Miyamoto, Tetsuya Taketsugu and Takeshi Iwasa

The Journal of Chemical Physics ARTICLE scitation.org/journal/jcp

A comparative study of structural, electronic, and optical properties of thiolated gold clusters with icosahedral vs face-centered cubic cores

Cite as: J. Chem. Phys. 155, 094304 (2021); doi: 10.1063/5.0057566
Submitted: 22 May 2021 • Accepted: 17 August 2021 •
Published Online: 2 September 2021

Maho Miyamoto,[1] Tetsuya Taketsugu,[2,3,4] and Takeshi Iwasa[2,3,4,a)]

AFFILIATIONS

[1] Graduate School of Chemical Sciences and Engineering, Hokkaido University, Sapporo 060-0810, Japan
[2] Department of Chemistry, Faculty of Science, Hokkaido University, Sapporo 060-0810, Japan
[3] WPI-ICReDD, Hokkaido University, Sapporo 001-0021, Japan
[4] ESICB, Kyoto University, Kyoto 615-8245, Japan

Note: This paper is part of the JCP Special Topic on From Atom-Precise Nanoclusters to Superatom Materials.
[a)] **Author to whom correspondence should be addressed:** tiwasa@sci.hokudai.ac.jp

ABSTRACT

The structural, electronic, and optical properties of the protected Au clusters with icosahedral (Ih) and face-centered cubic (FCC)-like Au_{13} cores were studied to understand the origin of the difference in the optical gaps of these clusters. It has been demonstrated that the choice of density functionals does not qualitatively affect the properties of Au_{23} and Au_{25} clusters with Ih and FCC cores. The density of states, molecular orbitals, and natural charges were analyzed in detail using the B3LYP functional. The substantial energy difference in the lowest-energy absorption peaks for the clusters with the Ih and FCC cores is attributed to the difference in the natural charges of the central Au atoms (Au_c) in the Ih and FCC cores, the former of which is more negative than the latter. Natural population analysis demonstrates that the excess negative charge of the Au_c atom in clusters with Ih cores occupies the 6*p* atomic orbitals. This difference in Au_c is attributed to the smaller size of the Ih core compared to the FCC core, as a less bulky ligand allows a smaller core with increased electron density, which, in turn, increases the highest occupied molecular orbital energy and decreases the optical gap.

I. INTRODUCTION

In recent decades, Au clusters protected by organic ligands have been extensively studied,[1–8] enabling precise chemical synthesis,[9–12] total structural determination,[13–16] and enhanced theoretical understanding.[16–20] Owing to their optical[16,21–24] and magnetic[25–27] properties and catalytic activities,[28–30] ligand-protected Au clusters are candidate materials for several applications. The most extensively studied system of this kind is $[Au_{25}(SR)_{18}]^-$, which is composed of an icosahedral (**Ih**) Au_{13} core and six Au–thiolate complexes of $Au_2(SR)_3$, hereafter called staples.[16,31] The superatom view successfully explains its physical properties, including its high stability.[19]

The superatom model was developed to explain the stability of a series of stable Na clusters in terms of their atom-like electronic shell closings.[32–34] The superatomic electronic shell is described by a spherical jellium model in which the electronic structure is similar to that of atoms but with different orders of electronic levels, such as 1*s*, 1*p*, 1*d*, and 2*s*.[32,33] This model underlies the physics of magic-numbered atomic clusters.[13,19,35,36] The superatom view was found to apply to ligand-protected clusters, in addition to bare pure- and mixed-metal clusters.

In $[Au_{25}(SR)_{18}]^-$, eight of the 13 6*s* electrons of the Au atoms in the metal core are delocalized to form the $1S^2 1P^6 1D^0$ superatomic shell closing, while the other 6*s* electrons are trapped to form Au_{13}–S bonds. Following this convention, we use capital letters for superatom orbitals. The lowest unoccupied molecular orbital (LUMO) of the *D* shell is split by the staple ligand field.[37,38] In addition to its stability, the optical properties of the system can be clearly understood with these superatom orbitals, as the lowest-lying excited states are

P–*D* transitions, where the doubly degenerate *D* orbitals are lower in energy after the ligand-field split, unlike those of conventional hexa-coordinated complexes.[16,31,38–41]

While $Au_{25}SR_{18}$ with an **Ih** core has been extensively studied, Negishi *et al.* reported in 2006 that the Au_{25} cluster passivated by the bulky thiol *N*-(2-mercaptopropionyl)glycine, called (PG)SH, showed an optical spectrum with a peak position substantially blue-shifted compared to that in the **Ih** cluster.[42] Recently, they revisited a higher-purity $Au_{25}(SPG)_{18}$ system.[43] Although its geometric structure still requires determination, they proposed two possible structures having $Au_{15}S_4$ cores in which a face-centered cubic (FCC)-like Au_{13} core is decorated by two thiols and two terminal Au atoms, as in the core + *exo* concept.[44] These two possible structures were derived based on the resemblance of the optical spectrum of $Au_{25}(SPG)_{18}$ to that of $Au_{23}(SR)_{16}$ (hereafter called **Au_{23}**) synthesized previously by Das *et al.*[45] The structure of **Au_{23}** is fully resolved, with a center comprising $Au_{15}S_4$. The optical gap of **Au_{23}** is larger than that of **Ih**-Au_{25} and very close to that of $Au_{25}(SPG)_{18}$.[43] From the superatom perspective, Xiong *et al.* found that Au_{13} in the $Au_{15}S_4$ core has eight electrons with two Au_4^{2+} and two Au_2^{3+} ions having the orbital configuration $1S^2 1P^4 1D^2$.[46] The $Au_{15}S_4$ core was called mono-cuboctahedral and designated as "13 + 2" by Li *et al.*[47] From the superatomic point of view, the **FCC** core is not electronically closed but has larger optical gap energy than the electronically closed **Ih**-Au_{25}. This is counterintuitive. Superatomic analysis allows us to determine the qualitative stability but not the orbital energies or, therefore, the optical gap energy. Further theoretical studies are required to understand such core–property relationships.

Although the relative energies for possible isomers of $Au_{25}(SPG)_{18}$ have been studied by density functional theory (DFT) calculations, optical simulations have not yet been explored. Furthermore, the relationships between the core structure and optical properties remain unsolved.[43] Understanding the relationship between the structural and optical properties is essential for further research toward the development of ligand-protected cluster chemistry.

In this study, we have investigated the structural, electronic, and optical properties of Au_{25} clusters with **Ih** Au_{13} and FCC-$Au_{15}S_4$ (**FCC**) cores, as well as **Au_{23}** with FCC $Au_{15}S_4$ cores, with a particular focus on the structure–property relationships. For the **FCC** Au_{25} cluster, Tsukuda *et al.* compared four structures, termed in their paper as **A**, **B**, **G**, and **N**, with **Ih**. We begin by studying these four structures, called **FCC1–4** in this paper, and continue by comparing the absorption spectra of **FCC1–4** with those of **Au_{23}** to determine the feasible isomers. Subsequently, a detailed comparative study of the structural, electronic, and optical properties of clusters with **Ih** and **FCC** cores was performed.

II. COMPUTATIONAL DETAILS

All density functional computations were performed with TURBOMOLE[48,49] under the resolution of identity (RI) approximation using the def-SV(P) basis sets[50] along with the 60-electron relativistic effective core potentials for Au[51] for the generalized gradient approximation (GGA) functional of BP86,[52,53] hybrid functionals of B3LYP[54,55] and PBE0,[56,57] and a range-separated functional of CAM-B3LYP.[58] The electronic absorption spectra were simulated in the framework of time-dependent DFT (TDDFT),[59–62] in which the line spectra were convoluted by a Lorentz function with a width of 0.05 eV.

III. RESULTS AND DISCUSSION

A. Ih and Au_{23}

We first checked the functional dependencies of the **Ih** and **Au_{23}** results. There are a number of theoretical studies on **Ih**; meanwhile, the DFT studies of **Au_{23}** and **FCC1–4** are relatively scarce. In this paper, we study the functional dependencies of these clusters for future reference. From the DFT studies of **Ih**, it is recognized that the qualitative picture of the structural, electronic, and optical properties is almost unchanged upon changing the functionals from GGA to hybrid types. Quantitatively, there is a known trend in the simulated optical gap energy in the order of GGA < hybrid functionals.[39–41]

Figure 1 shows the experimental and optimized structures of **Ih** and **Au_{23}**, as well as their representative interatomic distances. The Au–S frameworks are shown for the experimental geometries, as the remaining parts are bulky and difficult to compare with the computational results. The optimized structure of **Ih** with PBE0 shows a small imaginary frequency of −7.72 cm^{-1}; however, the following discussions are unaffected by its presence, as it is close to a true minimum. As shown in Figs. 1(a)–1(j), the functional dependencies on the structure were very small. From the interatomic distance distributions shown in Figs. 1(k) and 1(l), the theoretically

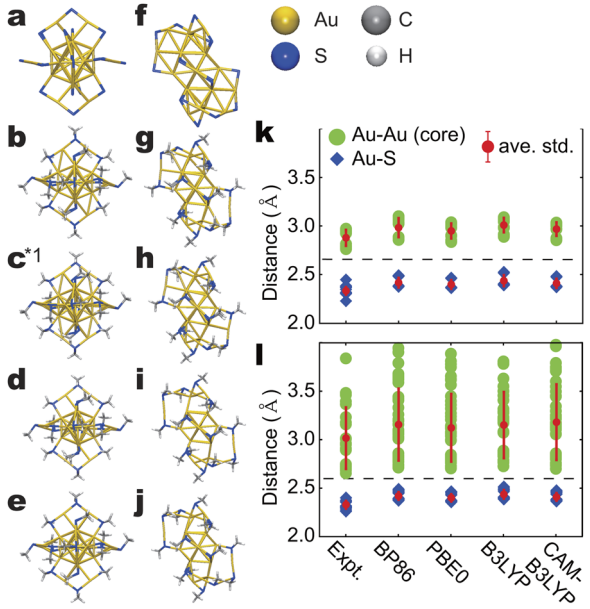

FIG. 1. (a) Experimental and optimized structures of the **Ih** cluster with (b) BP86, (c) PBE0, (d) B3LYP, and (e) CAM-B3LYP functionals and (f)–(j) those of the **Au_{23}** cluster. Color labels for Au, S, C, and H atoms are shown in the top right. Chosen interatomic distances and their average and standard deviations for (k) **Ih** and (l) **Au_{23}** clusters are shown. *1A small imaginary frequency is found at −7.72 cm^{-1}, mostly attributed to C and H atoms.

optimized distances were longer than those of the experiment. Au–S distances are localized around 2.4 Å. The Au–Au distances within the Au_{13} and $Au_{15}S_4$ cores (shown later in Fig. 7), depicted in red, are well localized for Au_{13}, as in the experiments. Overall, the differences are very small among the functionals used, but it seems that PBE0 and CAM-B3LYP yield predicted distances that are close to the experimental results, while those from BP86 and B3LYP are slightly longer.

Figure 2 shows the computed absorption spectra of **Ih** and **Au_{23}** with different functionals. The experimental absorption peak positions are shown by the vertical dashed lines to allow the comparison of the calculated and experimental peak positions. For **Ih**, as already known, BP86 (GGA) underestimates the excitation energy; this is overcome by the hybrid functionals PBE0 and B3LYP, including the Hartree–Fock exchange term. For **Au_{23}**, the hybrid functionals slightly overestimate the excitation energy. For both clusters, the range-separated functional (CAM-B3LYP) largely overestimates the excitation energy in these clusters. For **Ih**, the CAM-B3LYP result seems poor even qualitatively, as it shows three distinct peaks, while the others show one sharp peak in the lowest-energy region, followed by the higher-energy excited states that are energetically separated from the lowest-energy peak by ~1 eV. The long-range correction would work for clusters with larger ligands, such as those used in the experiments, because some of the low-lying excited states could have a signature of metal-to-ligand charge transfer. The theoretical and experimental spectral matches were good with PBE0 and B3LYP for **Ih**. For **Au_{23}**, the BP86 results seemed good, while PBE0 and B3LYP still exhibited similar spectral patterns.

B. FCC-Au_{25} cluster

As stated above, the Au_{25} cluster protected by bulky ligands (SPG) is expected to have an FCC core. We examined the four structures proposed by Omoda *et al.*,[43] two of which (**FCC1** and **FCC2**) have $Au_{15}S_4$ cores with FCC-like cuboctahedral arrangements. **FCC3** and **FCC4** have Au_7 planar cores, as we proposed previously.[17,63] **FCC1** consists of an $Au_{15}S_4$ core protected by two $Au_2(SR)_3$ and two $Au_3(SR)_4$ groups, while **FCC2** has a core protected by two $AuSR_2$ and two Au_4SR_5 groups. **FCC3** and **FCC4** consist of planar Au_7 + Au–S rings and two Au_3SR_3 + $Au_{12}SR_{12}$ rings. The stabilities of these four isomers and **Ih** were studied with B3LYP using the basis sets of LanL2DZ(Au) and 6-31G*(S, C, H) with Gaussian09. Together with the fragmentation pattern in the mass spectrum, Omoda *et al.* concluded that **FCC1 (A)** is the most probable structure; however, they did not compare the ultraviolet-visible (UV-vis) spectra. In this study, we studied the optical properties of these five structures. Figure 3 shows the optimized structures of **FCC1–4** obtained previously and in this study with the BP86, PBE0, B3LYP, and CAM-B3LYP functionals. The interatomic distances are also shown. As with **Ih** and **Au_{23}**, these structures are independent of the functionals. In addition, the bond lengths are longer in the simulations using B3LYP and CAM-B3LYP than in those using BP86 and PBE0.

The relative energies of **FCC1–4** with respect to **Ih** are summarized in Table I. Our results are partly consistent with those of a previous study. The relative energies of **FCC1** and **FCC2** are similar, and those of **FCC3** and **FCC4** are much higher for all functionals used. However, the stabilities of **FCC1** and **FCC2** relative to those of **Ih** vary depending on the function. B3LYP shows equal stability regardless of the computational software and a small difference in the functional: B3LYP in Gaussian09 adopts Vosko–Wilk–Nusair[64] (VWN) type III, while TURBOMOLE uses type V. For BP86 and PBE0, these two **FCC** structures have higher energies than **Ih**, while for CAM-B3LYP, the energies are similar.

Figure 4 compares the computed absorption spectra of **FCC1–4** with those of **Au_{23}**. The spectra of **FCC3** and **FCC4** differ significantly from those of **Au_{23}**. Together with the energetic results, these two isomers can be ruled out as candidate structures for FCC Au_{25}.

FCC1 and **FCC2** show absorption onsets and peak positions similar to those of **Au_{23}**, with energies larger than those of **Ih**. This trend is consistent with the experimental findings. With BP86, the first peak is not very prominent for **FCC1** compared to that for **FCC2**. In addition, with B3LYP, the second peak for **FCC1** appears

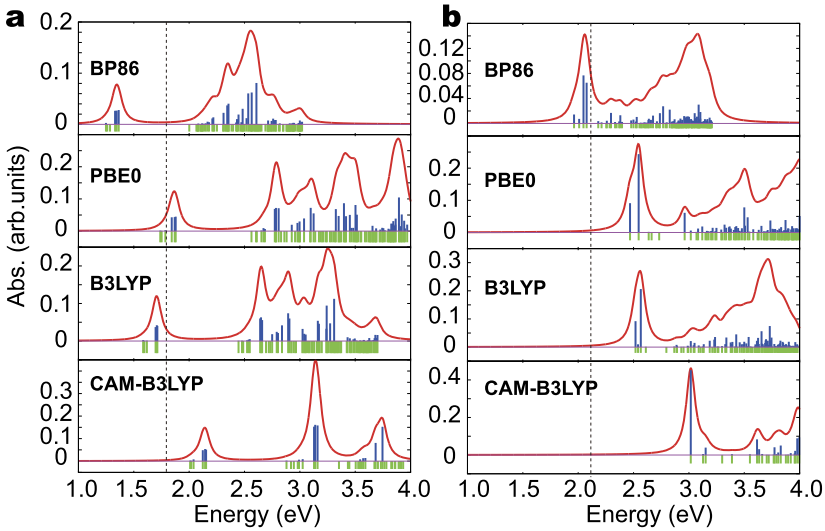

FIG. 2. Computed absorption spectra of (a) **Ih** and (b) **Au_{23}** with the functionals indicated inside. Green lines show the position of excited states, and oscillator strengths are shown by blue lines. The red curves are obtained by convoluting the oscillator strength with Lorentz functions. Dashed lines indicate the position of experimental absorption peaks.[43]

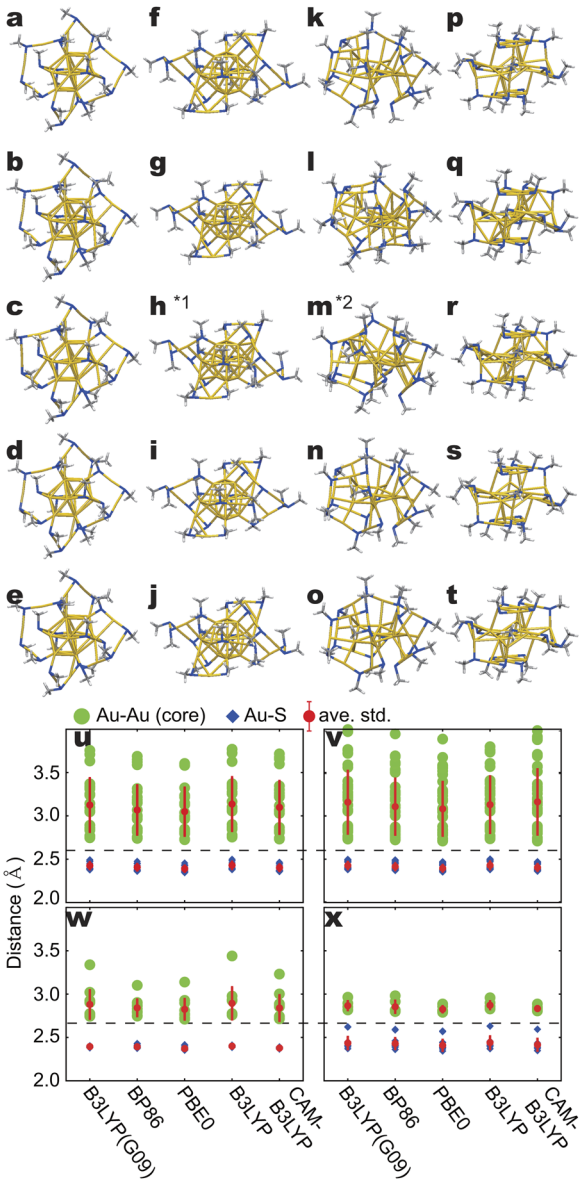

FIG. 3. Optimized structures of (a)–(e) **FCC1**, (f)–(j) **FCC2**, (k)–(o) **FCC3**, and (p)–(t) **FCC4** with (a), (f), (k), and (p) B3LYP with Gaussian09,[43] (b), (g), (l), and (q) BP86, (c), (h), (m), and (r) PBE0, (d), (i), (n), and (s) B3LYP, and (e), (j), (o), and (t) CAM-B3LYP. Small imaginary frequencies appear around CH_3: *1 (-2.54 cm^{-1}) and *2 (-1.21 cm^{-1}). The Au–Au distances within the core, Au–S distances, and their average and standard deviations are shown by green circles, blue rhombuses, and red circles and bars, respectively, for (u) **FCC1**, (v) **FCC2**, (w) **FCC3**, and (x) **FCC4**.

just after the first. From this spectroscopic viewpoint, **FCC2** seems better than **FCC1**, although the structures show similar features. Both are used for the remainder of this paper to investigate the relationship between the core geometry and electronic and optical properties. We hereafter use B3LYP. Our previous studies on the optical properties of ligand-protected Au clusters have shown that B3LYP yields reasonable results.[18,41,44,65]

TABLE I. Relative total energies in eV for **FCC1–4** with reference to **Ih**.

	B3LYP[a]	BP86	PBE0	B3LYP	CAM-B3LYP
FCC1	−0.3	+0.50	+0.90	−0.38	−0.02
FCC2	−0.3	+0.57	+1.14	−0.34	+0.18
FCC3	+1.9	+2.89	+4.12	+2.06	+3.47
FCC4	+3.0	+3.57	+4.86	+3.30	+4.49

[a]B3LYP/LanL2DZ(Au), 6-31G*(S, C, H) with Gaussian09.[43]

C. Comparative study of Ih, FCC, and Au_{23}

In the following, we attempt to determine the relationship between the core geometry and the electronic and optical properties.

1. Excited states concerning the absorption onset

As shown in Figs. 2 and 4, **FCC1/2** and **Au_{23}** show absorption peaks around 2.5 eV, which is higher than that of **Ih** (~1.7 eV). This is the same trend observed experimentally, but the energy difference is slightly larger in our B3LYP results. Although quantitative improvements remain possible, our computations reproduce the substantial peak shift to higher energy from **Ih** to **FCC** and **Au_{23}**. The lowest-energy peak of **Ih** consists of the excited states of S_4–S_6. As shown in Fig. 5(a), these excited states are attributed to the transition from the triply degenerate superatomic $P_{x/y/z}$ orbitals to doubly degenerate D_{x2-y2} and D_{z2} orbitals, consistent with previous reports.[16,40,41] Meanwhile, **FCC1**, **FCC2**, and **Au_{23}** have the $Au_{15}S_4$ core, which is non-spherical with lower symmetry than the **Ih** core. The order of the superatom orbitals changes with a decrease in the cluster symmetry.[46,66] While Das *et al.* performed TDDFT calculations with PBE0 and stated that the **Au_{23}** cluster is non-superatomic,[45] these orbitals can be seen as a transition from D_{z2} to F_{z2} for a single superatom or from $P_z\sigma$ to $P_z\sigma^*$ in a superatom dimer. These orbitals are also found in our calculations, as shown in Fig. 5(b), as the transition from the highest occupied molecular orbital (HOMO; H) to the LUMO (L). The transition from H to LUMO + 1 (L1) resembles the *D*–*P* transition. The superatomic perspective for **FCC1** and **FCC2** is also applicable. For **FCC1** shown in Fig. 5(c), H1–L and H–L1 transitions are similar in nature to *P*–*D* and *D*–*F* transitions, whereas for **FCC2** shown in Fig. 5(d), H1–L and H–L can be seen as similar to localized *P* (to one side of the cluster) to *F* transitions in nature. While clear assignments are not easy for these lower-symmetry clusters, all these orbitals consist of the 6*s* and 6*p* atomic orbitals of Au delocalized over the cluster for all clusters studied in this paper, invoking the term pseudo-free electron.

In the following, we investigate the electronic structures of these clusters to elucidate the difference between the absorption peak positions of the **Ih** and **FCC** cores.

2. Density of states

Figure 6 shows the density of states (DOS) near the HOMO and LUMO, projected to Au (center), or Au_c, and Au (others) in the

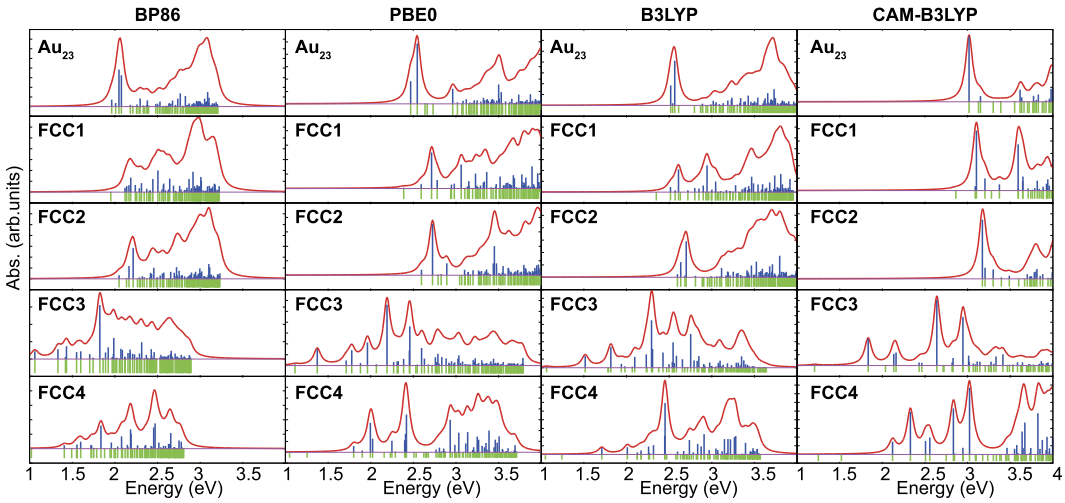

FIG. 4. Computed absorption spectra of **FCC1–4** compared with those of **Au_{23}** with different functionals. See Fig. 2 for further details on the colored lines and curves.

core and other atoms, as shown in the inset. The position of Au_c is shown in Fig. 7. The DOS is obtained based on Mulliken population analysis (MPA). It is known that MPA sometimes provides negative contributions.[67] Indeed, some components are negative in this study, making the DOS shown in Fig. 7 less quantitative. As an example, Fig. 5(a) shows that the HOMO of **Ih** is delocalized in the cluster, while Fig. 6(a) shows that the HOMO is highly localized to Au_c. This discrepancy originates from the negative population in the MPA. In detail, some of the Au atomic orbitals in the Au_{13} core have negative populations that cancel the positive populations of the other Au atomic orbitals, thus artificially enlarging Au_c. Therefore, the DOSs are not very quantitative, but they indicate the overall distributions of the Kohn–Sham (KS) orbitals and their components in a wider energy range. We used the DOS to determine the overall behavior of the electronic structures of these clusters.

As shown in Fig. 6, the HOMO–LUMO gap energy is larger for **FCC** and **Au_{23}** than for **Ih** by ~1 eV. For all the clusters, the LUMO is commonly positioned around −0.4 eV. In sharp contrast,

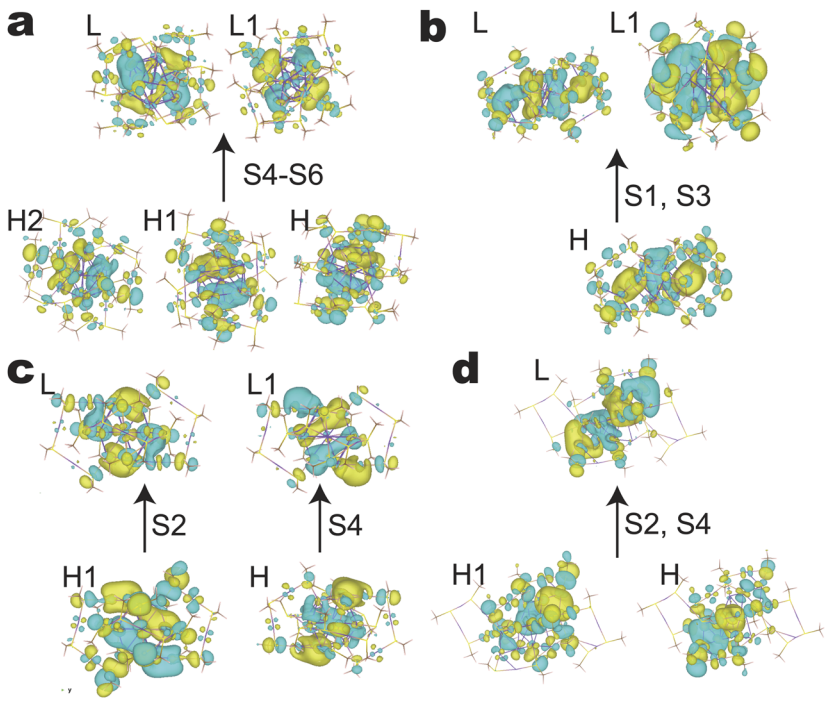

FIG. 5. KS orbitals relating to the lowest absorption peaks of (a) **Ih**, (b) **Au_{23}**, (c) **FCC1**, and (d) **FCC2** clusters calculated with the B3LYP functional. HOMO − 2 to LUMO + 1 are labeled as H2, H1, H, L, and L1 in this figure; the respective excited states are shown next to arrows.

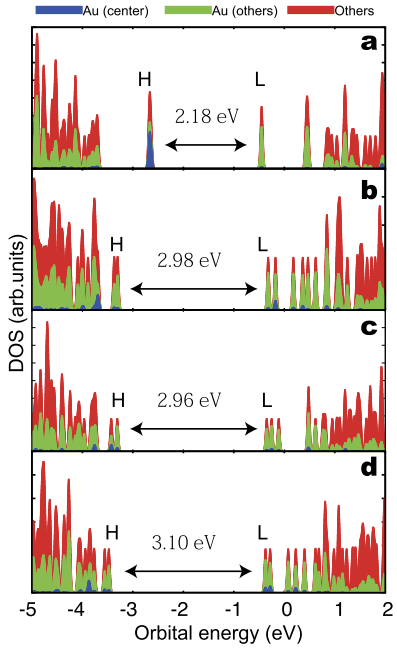

FIG. 6. Density of states for (a) **Ih**, (b) **Au_{23}** (c) **FCC1**, and (d) **FCC2** clusters calculated with the B3LYP functional. Blue and green denote the contributions from Au_c and other Au atoms in the core, and red denotes those from other atoms, such as Au in ligands, S, C, and H. HOMO (H), LUMO (L), and their gap energies are also indicated.

the HOMO energies vary significantly. For **Ih**, it is around −2.6 eV, but it is around −3.4 eV for **FCC** and **Au_{23}**. From the DOS, the large energy gap difference between the **Ih** and **FCC** cores could be understood by inspecting the HOMO, leading to a change in the peak position in the absorption spectra.

From the projection of DOS to Au_c and other Au atoms, the HOMO is strongly affected by Au_c in the **Ih** core. For the other clusters, Au_c does not strongly contribute to the HOMO. The natural charges of these Au_cs are listed in Table II. The natural charge is largely negative for **Ih** (−0.41) and moderate for the others (−0.14 to −0.16). As the atomic/molecular orbitals of negatively charged species are generally higher in energy than their counterparts in more positively charged states, the HOMO of **Ih** has a higher energy than the others. In addition, the natural configuration of Au_c for **Ih** has a 6*p* orbital population approaching 0.5, while that for the others is ~0.1. The HOMO of **Ih** is superatomic *P* in character, and the central atoms should have the same node and lobe, leading to a larger 6*p* population than the others. All these factors partially contribute to the increase in the HOMO energy of **Ih** compared to that of the others.

TABLE II. Natural charges (NC) of the central Au and distances from Au_c for **Ih**, **FCC1**, **FCC2**, and **Au_{23}** clusters calculated with B3LYP.

	NC	Au_c–Au (Å)
Ih	−0.41	2.89–2.91
Au_{23}	−0.15	2.83–2.89, 3.28–3.29, 3.41–3.63
FCC1	−0.14	2.86–2.90, 3.26–3.28, 3.63–3.72
FCC2	−0.16	2.83–2.90, 3.26–3.32, 3.40–3.61

3. Close examination of core geometry

In addition to the natural charges, the distances from Au_c to the surrounding Au atoms are also given in Table II. For **FCC1** and **FCC2**, the distances from Au_c to the two terminal Au atoms are omitted because they are larger than 4 Å. For Au_{13}, all the distances from Au_c to the 12 surface Au atoms are ~2.90 Å. The distances in the $Au_{15}S_4$ core are classified into three groups. The short Au–Au distances are localized at 2.83–2.90 Å, similar to or shorter than those of the Au_{13} core. The intermediate and longer distances are 3.26–3.32 and 3.4–3.7 Å, substantially exceeding those of the Au_{13} core. Furthermore, the **FCC** core contains four negatively charged S atoms. These negative charges can lead to the enlargement of the core through Coulomb repulsion. For these reasons, the **FCC** core is larger than the **Ih** core; therefore, the **FCC** atomic and electron densities are smaller. Conversely, the electron density for the **Ih** core is larger, leading to an increase in the orbital energy. This core size difference causes electron density distributions, leading to differences in the HOMO–LUMO gap energies and, therefore, in the optical gaps.

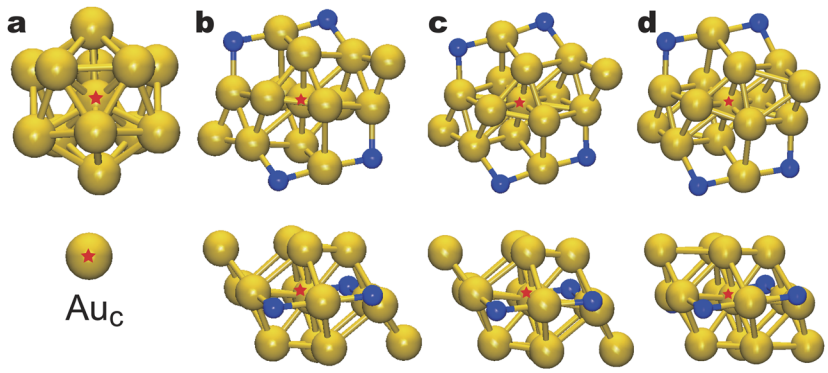

FIG. 7. Au_{13} core geometries of (a) **Ih** and $Au_{15}S_4$ of (b) **Au_{23}**, (c) **FCC1**, and (d) **FCC2** clusters calculated with the B3LYP functional. Au_c is indicated by a red star.

IV. CONCLUSIONS

In summary, we have studied two different types of Au clusters, one of which has an **Ih** Au_{13} core and the other has an **FCC**-like $Au_{15}S_4$ core, with the aim of elucidating the relationship between the core structures and the electronic and optical properties of the clusters. The clusters synthesized with bulky ligands have larger cores than those with less bulky ligands. The smaller cores have increased electron densities and unexpectedly high molecular orbital energies. This results in differences in the onset of optical absorption between the two cluster types. This is supported by the prominent difference in the natural charge and the 6*p* population of the central Au atoms.

The simulated structural, electronic, and optical properties are qualitatively insensitive to the functionals used for prediction. Quantitatively, the optical gap energy is generally small in GGA and large in functionals that explicitly incorporate the Hartree–Fock exchange integral. A balanced description of the present clusters was obtained using hybrid functionals, such as B3LYP and PBE0. It was found that the use of the LC functional overestimates the optical energies; however, such a functional can be essential for clusters with excited states having a charge-transfer nature, such as metal-to-ligand or vice versa. In contrast to these moderate variations, we have shown that the cluster stability can depend on the functionals even qualitatively, suggesting the importance of cross-checking with several functionals.

Finally, our spectroscopic comparisons of **FCC** with $\mathbf{Au_{23}}$ show that the overall shape of the experimental spectrum is better matched for **FCC2** than for **FCC1**, but not exclusively so. These two isomers are energetically similar, with the possibility of coexistence. This should be investigated in the future by single-crystal x-ray diffraction.

ACKNOWLEDGMENTS

We thank Professor Andrey Lyalin and Dr. Sonu Kumar for their critical reading of our manuscript and valuable suggestions. T.I. acknowledges the financial support provided by the Japan Society for the Promotion of Science (JSPS) KAKENHI (Grant Nos. JP20K05412, JP20H04652, and JP20K05592) and the Institute for Quantum Chemical Exploration. This work was also partly supported by the Elements Strategy Initiative of MEXT (Grant No. JPMXP0112101003), the Photoexcitonix Project at Hokkaido University, and JST CREST, Japan (Grant No. JPMJCR1902).

DATA AVAILABILITY

The data that support the findings of this study are available from the corresponding author upon reasonable request.

REFERENCES

[1] A. C. Templeton, W. P. Wuelfing, and R. W. Murray, Acc. Chem. Res. **33**, 27 (2000).
[2] M.-C. Daniel and D. Astruc, Chem. Rev. **104**, 293 (2004).
[3] H. Häkkinen, Chem. Soc. Rev. **37**, 1847 (2008).
[4] R. Sardar, A. M. Funston, P. Mulvaney, and R. W. Murray, Langmuir **25**, 13840 (2009).
[5] J. F. Parker, C. A. Fields-Zinna, and R. W. Murray, Acc. Chem. Res. **43**, 1289 (2010).
[6] R. Jin, Nanoscale **2**, 343 (2010).
[7] R. Jin, C. Zeng, M. Zhou, and Y. Chen, Chem. Rev. **116**, 10346 (2016).
[8] H. Hirai, S. Ito, S. Takano, K. Koyasu, and T. Tsukuda, Chem. Sci. **11**, 12233 (2020).
[9] R. C. Price and R. L. Whetten, J. Am. Chem. Soc. **127**, 13750 (2005).
[10] Y. Negishi, K. Nobusada, and T. Tsukuda, J. Am. Chem. Soc. **127**, 5261 (2005).
[11] W. Kurashige, Y. Niihori, S. Sharma, and Y. Negishi, Coord. Chem. Rev. **320–321**, 238 (2016).
[12] Y. Negishi, S. Hashimoto, A. Ebina, K. Hamada, S. Hossain, and T. Kawawaki, Nanoscale **12**, 8017 (2020).
[13] P. D. Jadzinsky, G. Calero, C. J. Ackerson, D. A. Bushnell, and R. D. Kornberg, Science **318**, 430 (2007).
[14] Y. Shichibu, Y. Negishi, T. Watanabe, N. K. Chaki, H. Kawaguchi, and T. Tsukuda, J. Phys. Chem. C **111**, 7845 (2007).
[15] M. W. Heaven, A. Dass, P. S. White, K. M. Holt, and R. W. Murray, J. Am. Chem. Soc. **130**, 3754 (2008).
[16] M. Zhu, C. M. Aikens, F. J. Hollander, G. C. Schatz, and R. Jin, J. Am. Chem. Soc. **130**, 5883 (2008).
[17] T. Iwasa and K. Nobusada, J. Phys. Chem. C **111**, 45 (2007).
[18] K. Nobusada and T. Iwasa, J. Phys. Chem. C **111**, 14279 (2007).
[19] M. Walter, J. Akola, O. Lopez-Acevedo, P. D. Jadzinsky, G. Calero, C. J. Ackerson, R. L. Whetten, H. Gronbeck, and H. Hakkinen, Proc. Natl. Acad. Sci. U. S. A. **105**, 9157 (2008).
[20] D.-E. Jiang, S. H. Overbury, and S. Dai, J. Am. Chem. Soc. **135**, 8786 (2013).
[21] T. G. Schaaff and R. L. Whetten, J. Phys. Chem. B **104**, 2630 (2000).
[22] T. P. Bigioni, R. L. Whetten, and Ö. Dag, J. Phys. Chem. B **104**, 6983 (2000).
[23] T. Huang and R. W. Murray, J. Phys. Chem. B **105**, 12498 (2001).
[24] M. Y. Sfeir, H. Qian, K. Nobusada, and R. Jin, J. Phys. Chem. C **115**, 6200 (2011).
[25] Y. Yamamoto, T. Miura, M. Suzuki, N. Kawamura, H. Miyagawa, T. Nakamura, K. Kobayashi, T. Teranishi, and H. Hori, Phys. Rev. Lett. **93**, 116801 (2004).
[26] P. Crespo, R. Litrán, T. Rojas, M. Multigner, J. de la Fuente, J. Sánchez-López, M. García, A. Hernando, S. Penadés, and A. Fernández, Phys. Rev. Lett. **93**, 087204 (2004).
[27] J. de la Venta, A. Pucci, E. Fernández Pinel, M. A. García, C. de Julián Fernandez, P. Crespo, P. Mazzoldi, G. Ruggeri, and A. Hernando, Adv. Mater. **19**, 875 (2007).
[28] H. Tsunoyama, H. Sakurai, N. Ichikuni, Y. Negishi, and T. Tsukuda, Langmuir **20**, 11293 (2004).
[29] H. Tsunoyama, H. Sakurai, Y. Negishi, and T. Tsukuda, J. Am. Chem. Soc. **127**, 9374 (2005).
[30] G. Li and R. Jin, Acc. Chem. Res. **46**, 1749 (2013).
[31] J. Akola, M. Walter, R. L. Whetten, H. Häkkinen, and H. Grönbeck, J. Am. Chem. Soc. **130**, 3756 (2008).
[32] W. D. Knight, K. Clemenger, W. A. de Heer, W. A. Saunders, M. Y. Chou, and M. L. Cohen, Phys. Rev. Lett. **52**, 2141 (1984).
[33] W. Ekardt, Phys. Rev. B **29**, 1558 (1984).
[34] X. Li, H. Wu, X.-B. Wang, and L.-S. Wang, Phys. Rev. Lett. **81**, 1909 (1998).
[35] J. U. Reveles, S. N. Khanna, P. J. Roach, and A. W. Castleman, Proc. Natl. Acad. Sci. U. S. A. **103**, 18405 (2006).
[36] P. Jena, J. Phys. Chem. Lett. **4**, 1432 (2013).
[37] C. M. Aikens, J. Phys. Chem. C **112**, 19797 (2008).
[38] C. M. Aikens, J. Phys. Chem. Lett. **2**, 99 (2011).
[39] D.-e. Jiang, M. Kühn, Q. Tang, and F. Weigend, J. Phys. Chem. Lett. **5**, 3286 (2014).
[40] K. L. D. M. Weerawardene and C. M. Aikens, J. Am. Chem. Soc. **138**, 11202 (2016).
[41] M. Ebina, T. Iwasa, Y. Harabuchi, and T. Taketsugu, J. Phys. Chem. C **122**, 4097 (2018).
[42] Y. Negishi, Y. Takasugi, S. Sato, H. Yao, K. Kimura, and T. Tsukuda, J. Phys. Chem. B **110**, 12218 (2006).
[43] T. Omoda, S. Takano, S. Yamazoe, K. Koyasu, Y. Negishi, and T. Tsukuda, J. Phys. Chem. C **122**, 13199 (2018).

[44]Y. Shichibu, M. Zhang, T. Iwasa, Y. Ono, T. Taketsugu, S. Omagari, T. Nakanishi, Y. Hasegawa, and K. Konishi, J. Phys. Chem. C **123**, 6934 (2019).
[45]A. Das, T. Li, K. Nobusada, C. Zeng, N. L. Rosi, and R. Jin, J. Am. Chem. Soc. **135**, 18264 (2013).
[46]L. Xiong, S. Yang, X. Sun, J. Chai, B. Rao, L. Yi, M. Zhu, and Y. Pei, J. Phys. Chem. C **122**, 14898 (2018).
[47]Q. Li, M. Zhou, W. Y. So, J. Huang, M. Li, D. R. Kauffman, M. Cotlet, T. Higaki, L. A. Peteanu, Z. Shao, and R. Jin, J. Am. Chem. Soc. **141**, 5314 (2019).
[48]TURBOMOLE V7.5, A development of University of Karlsruhe and Forschungszentrum Karlsruhe GmbH, 1989–2007, TURBOMOLE GmbH, since 2007, available at http://www.turbomole.com.
[49]R. Ahlrichs, M. Bär, M. Häser, H. Horn, C. Kölmel, H. Marco, H. Horn, and C. Kölmel, Chem. Phys. Lett. **162**, 165 (1989).
[50]A. Schäfer, H. Horn, and R. Ahlrichs, J. Chem. Phys. **97**, 2571 (1992).
[51]D. Andrae, U. Häussermann, M. Dolg, H. Stoll, and H. Preuss, Theor. Chim. Acta **77**, 123 (1990).
[52]J. P. Perdew, Phys. Rev. B **33**, 8822 (1986).
[53]A. D. Becke, Phys. Rev. A **38**, 3098 (1988).
[54]C. Lee, W. Yang, and R. G. Parr, Phys. Rev. B **37**, 785 (1988).
[55]A. D. Becke, J. Chem. Phys. **98**, 1372 (1993).
[56]J. P. Perdew, K. Burke, and M. Ernzerhof, Phys. Rev. Lett. **77**, 3865 (1996).
[57]J. P. Perdew, M. Ernzerhof, and K. Burke, J. Chem. Phys. **105**, 9982 (1996).
[58]T. Yanai, D. P. Tew, and N. C. Handy, Chem. Phys. Lett. **393**, 51 (2004).
[59]M. E. Casida, *Recent Advances in Density Functional Methods Part I*, edited by D. P. Chong (World Scientific, Singapore, 1995).
[60]R. Bauernschmitt and R. Ahlrichs, Chem. Phys. Lett. **256**, 454 (1996).
[61]R. Bauernschmitt, M. Häser, O. Treutler, and R. Ahlrichs, Chem. Phys. Lett. **264**, 573 (1997).
[62]F. Furche, J. Chem. Phys. **114**, 5982 (2001).
[63]T. Iwasa and K. Nobusada, Chem. Phys. Lett. **441**, 268 (2007).
[64]S. H. Vosko, L. Wilk, and M. Nusair, Can. J. Phys. **58**, 1200 (1980).
[65]T. Iwasa, K. Nobusada, and A. Nakajima, J. Phys. Chem. C **117**, 24586 (2013).
[66]T. Omoda, S. Takano, and T. Tsukuda, Small **17**, 2001439 (2020).
[67]F. Jensen, *Introduction to Computational Chemistry*, 3rd ed. (John Wiley & Sons, West Sussex, 2017).